Isovalent Gold(I), -(II), and -(III) and Mixed-Valent Gold(I)/Gold(III) Phosphorus Ylide Complexes. Combined ab Initio and Density Functional Study of Electronic Structures and Spectroscopic Properties

Qing-Jiang Pan,[†] Xin Zhou,[‡] Hong-Gang Fu,*[,†] and Hong-Xing Zhang*[,‡]

Laboratory of Physical Chemistry, School of Chemistry and Materials Science, Heilongjiang University, Harbin 150080, People's Republic of China, and State Key Laboratory of Theoretical and Computational Chemistry, Institute of Theoretical Chemistry, Jilin University, Changchun 130023, People's Republic of China

Received November 5, 2007

The binuclear gold phosphorus ylide complexes $[Au^I_2(CH_2PH_2CH_2)_2]$ (**1**), $[Au^{II}_2X_2(CH_2PH_2CH_2)_2]$ (X = Cl (**2a**), Br (**2b**), I (**2c**)), $[Au^{III}_2X_4(CH_2PH_2CH_2)_2]$ (X = Cl (**3a**), Br (**3b**)), and $[Au^IAu^{III}X_2(CH_2PH_2CH_2)_2]$ (X = Cl (**4a**), Br (**4b**)) were explored using density functional theory and ab initio methods. The use of methods, basis sets, and substituent effects confirmed our calculations. The analyses on their electronic structures reveal that two- and four-electron oxidation from **1** to **2**−**4** mainly occurs at the gold centers, resulting in their different coordination geometry features and metal−metal interactions as well as spectroscopic properties. Bond-order and frequency calculations provided the evidence for the weak Au−Au bonding interaction in **1**, **3**, and **4** and an approximate Au−Au single bond in **2**. Unrestricted MP2 calculations showed that the triplet excited-state structures of **1**, **2a**, and **3a** are minimum points on the potential energy surface. Upon excitation, the Au−Au distances of **1** and **3a** shorten while that of **2a** increases. This is closely correlated with the promotion of electrons into the bonding or antibonding orbitals of the gold centers.

Introduction

Gold is a very special element and has some unique and even extreme chemical properties.[1–5] It displays different oxidation states, oxidation potentials, coordination numbers, and coordination geometries.[1–3] The molecular chemistry of gold is dominated by the complexes of the I and III oxidation states.[1,2] The former are generally found to be two-coordinate with a linear geometry of two donor atoms. In this kind of complex, two or more closed-shell Au^I cations, having distances slightly above that in gold metal, often form aggregates,[6] and the Au−Au bonding energies are comparable to that of a strong hydrogen bond,[6–8] despite the fact that both atoms carry charges of the same sign and have no valence electrons to make covalent bonds. However, the Au−Au single bond appears in bi- or polynuclear Au^{II} complexes because of the d^9-d^9 interactions. It was proved that these complexes exhibit a square-planar tetracoordination geometry.[9–11] Au^I, Au^{III}, and the rare Au^{II} cations are strong acceptors for nucleophiles. Their extreme Lewis acid behavior is perhaps most obvious from the spectacular finding that these cations can even bind the rare gas xenon in their first coordination sphere.[2a,8a] This has hitherto

* Corresponding authors. E-mail: fuhg@vip.sina.com; zhanghx@mail.jlu.edu.cn.

[†] Heilongjiang University.

[‡] Jilin University.

(1) Fackler, J. P., Jr *Inorg. Chem.* **2002**, *41*, 6959–6972.

(2) (a) Schmidbaur, H.; Cronje, S.; Djordjevic, B.; Schuster, O. *Chem. Phys.* **2005**, *311*, 151–161. (b) Schmidbaur, H. *Gold Bull.* **1990**, *23*, 11–21.

(3) (a) Pyykkö, P. *Angew. Chem., Int. Ed.* **2004**, *43*, 4412–4456. (b) Pyykkö, P. *Chem. Rev.* **1997**, *97*, 597–636.

(4) Gimeno, M C.; Laguna, A. *Chem. Rev.* **1997**, *97*, 511–522.

(5) (a) Yam, V. W.-W.; Chan, C. -L.; Li, C.-K.; Wong, K. M.-C. *Coord. Chem. Rev.* **2001**, *216*−*217*, 173–194. (b) Che, C.-M.; Lai, S.-W. *Coord. Chem. Rev.* **2005**, *249*, 1296–1309. (c) Phillips, D. L.; Che, C.-M.; Beung, K. H.; Mao, Z.; Tse, M.-C. *Coord. Chem. Rev.* **2005**, *249*, 1476–1490.

(6) (a) Mohamed, A. A.; Kani, I.; Ramirez, A. O.; Fackler, J. P., Jr *Inorg. Chem.* **2004**, *43*, 3833–3839. (b) van Zyl, W. E.; López-de-Luzuriaga, J. M.; Mohamed, A. A.; Staples, R. J.; Fackler, J. P., Jr *Inorg. Chem.* **2002**, *41*, 4579–4589. (c) Mansour, M. A.; Connick, W. B.; Lachicotte, R. J.; Gysling, H. J.; Eisenberg, R. *J. Am. Chem. Soc.* **1998**, *120*, 1329–1330. (d) Lee, Y. A.; McGarrah, J. E.; Lachicotte, R. J.; Eisenberg, R. *J. Am. Chem. Soc.* **2002**, *124*, 10662–10663. (e) Narayanaswamy, R.; Young, M. A.; Parkhurst, E.; Ouellette, M.; Kerr, M. E.; Ho, K. M.; Elder, R. C.; Bruce, A. E.; Bruce, M. R. M. *Inorg. Chem.* **1993**, *32*, 2506–2517. (f) Jones, W. B.; Yuan, J.; Narayanaswamy, R.; Young, M. A.; Elder, R. C.; Bruce, A. E.; Bruce, M. R. M. *Inorg. Chem.* **1995**, *34*, 1996–2001. (g) Schwerdtfeger, P.; Bruce, A. E.; Bruce, M. R. M. *J. Am. Chem. Soc.* **1998**, *120*, 6587–6597. (h) Rawashdeh-Omary, M. A.; Omary, M. A.; Patterson, H. H.; Fackler, J. P., Jr *J. Am. Chem. Soc.* **2001**, *123*, 11237–11247. (i) White-Morris, R. L.; Olmstead, M. M.; Balch, A. L. *J. Am. Chem. Soc.* **2003**, *125*, 1033. (j) White-Morris, R. L.; Olmstead, M. M.; Jiang, F.; Tinti, D. S.; Balch, A. L. *J. Am. Chem. Soc.* **2002**, *124*, 2327. (k) Olmsted, M. M.; Jiang, F.; Attar, S.; Balch, A. L. *J. Am. Chem. Soc.* **2001**, *123*, 3260. (l) Tang, S. S.; Chang, C.-P.; Lin, I. J. B.; Liou, L.-S.; Wang, J.-C. *Inorg. Chem.* **1997**, *36*, 2294–2300.

(7) (a) Pyykkö, P. *Science* **2000**, *290*, 64–65. (b) Pyykkö, P.; Runeberg, N.; Mendizabal, F. *Chem. Eur. J.* **1997**, *3*, 1451–1457. (c) Pyykkö, P.; Mendizabal, F. *Chem. Eur. J.* **1997**, *3*, 1458–1465. (d) Pyykkö, P.; Mendizabal, F. *Inorg. Chem.* **1998**, *37*, 3018–3025. (e) Pyykkö, P.; Schneider, W.; Bauer, A.; Bayler, A.; Schmidbaur, H. *Chem. Commun.* **1997**, 1111–1112.

(8) (a) Seidel, S.; Seppelt, K. *Science* **2000**, *290*, 117–118. (b) Pathaneni, S. S.; Desiraju, G. R. *J. Chem. Soc., Dalton Trans.* **1993**, 319–322.

(9) (a) Laguna, A.; Laguna, M. *Coord. Chem. Rev.* **1999**, *193*−*195*, 837–856. (b) Bardají, M.; Connelly, N. G.; Gimeno, C.; Jiménez, J.; Jones, P. G.; Laguna, A.; Laguna, M. *J. Chem. Soc., Dalton Trans.* **1994**, 1163–1167. (c) Bardají, M.; Connelly, N. G.; Gimeno, C.; Jones, P. G.; Laguna, A.; Laguna, M. *J. Chem. Soc., Dalton Trans.* **1995**, 2245–2250. (d) Bardají, M.; Laguna, A.; Laguna, M. *J. Organomet. Chem.* **1995**, *496*, 245–248.

10.1021/om701114z CCC: $40.75
Publication on Web 05/08/2008

not been observed for any other metal. These discoveries showed that the (multi)cations of gold, the most electronegative of the metals, are also the most powerful acceptors.[1–3]

A large number of complexes involving gold atoms in various oxidation states, bound by diverse ligands, have been synthesized and structurally characterized.[1,4–14] Special attention has been focused on the binuclear gold phosphorus ylides.[14–18] The oxidation of the binuclear Au^I ylide $[Au_2(CH_2PR_2CH_2)_2]$ (R = alkyl, aryl) with X_2 (X = Cl, Br) occurs stepwise to give Au^{II} and Au^{III} products. The structures of these complexes have been confirmed for a variety of alkyl substituents and halogens. Upon oxidation of gold from I to II to III, the Au−Au distance changes from 3.0 to 2.6 to 3.1 Å.[15–18] An interesting aspect of the chemistry of binuclear Au^{III} tetrahalide species is their two-electron reduction, which can lead to Au^{II} products or mixed-valence Au^I/Au^{III} species, depending on the reducing agent.[18–21] Additionally, the isomerization of the isoelectronic Au^{II}/Au^{II} and Au^I/Au^{III} complexes has been found through an intramolecular dis- or comproportionation process.[18,19] Despite their interesting structural and chemical properties, few theoretical studies have been attempted on the series of ylide complexes of gold in the I, II, and III oxidation states.[22]

At present, quantum chemistry methods are advanced and efficient enough to explore the electronic properties of transition-metal complexes.[23–26] It is possible to perform systematic theoretical studies on the electronic structures and spectroscopic properties of metal complexes. To understand the similarities and differences in the chemical properties of binuclear gold complexes with different oxidation states, we theoretically investigated the ground and excited states of $[Au^I_2(CH_2PH_2CH_2)_2]$ (**1**), $[Au^{II}_2X_2(CH_2PH_2CH_2)_2]$ (X = Cl (**2a**), Br (**2b**), I (**2c**)), $[Au^{III}_2X_4(CH_2PH_2CH_2)_2]$ (X = Cl (**3a**), Br (**3b**)) and $[Au^IAu^{III}X_2(CH_2PH_2CH_2)_2]$ (X = Cl (**4a**), Br (**4b**)). Spectroscopic properties, including vibrational and electronic spectra, are presented in the work.

Computational Details and Theory

In the calculations, we used an H atom to represent the R (R = Me, Et, Ph) group bonding to the real ligand ($CH_2PR_2CH_2$). This kind of simplification has been successfully applied in previous works.[3,6g,26] Here, we also performed the substituent-effect calculations on $[Au^I_2(CH_2PR_2CH_2)_2]$ (R = H (**1**), Me (**1-Me**), Ph (**1-Ph**)) to test the simplification.

We employed the second-order Møller−Plesset perturbation (MP2)[27] and density functional theory (XαVWN)[28] methods to optimize the structures of **1**−**4** in the ground states. It has been well-established that the transition energies calculated by the time-dependent density functional theory (TD-DFT) method are comparable in accuracy to those calculated by the higher-level configuration interaction methods.[23] On the basis of the ground-state structures of **1**−**4**, the TD-DFT method was used to predict the absorption spectra. Considering the influence of solvent molecules on the electronic spectroscopy of complexes, as indicated in the previous works,[24,26] we employed the polarized continuum

(10) (a) Murray, H. H.; Mazany, A. M.; Fackler, J. P., Jr *Organometallics* **1985**, *4*, 154–157. (b) Trzcinska-Bancroft, B.; Khan, M. N. I.; Fackler, J. P., Jr *Organometallics* **1988**, *7*, 993–996. (c) Khan, M. N. I.; Wang, S.; Fackler, J. P., Jr *Inorg. Chem.* **1989**, *28*, 3579–3588. (d) Calabro, D. C.; Harrison, B. A.; Pallmer, G. T.; Moguel, M. K. *Inorg. Chem.* **1981**, *20*, 4311–4316. (e) Fackler, J. P., Jr.; Basll, J. D. *Organometallics* **1982**, *1*, 871–873.

(11) Coetzee, J.; Gabrielli, W. F.; Coetzee, K.; Schuster, O.; Nogai, S. D.; Cronje, S.; Raubenheimer, H. G. *Angew. Chem., Int. Ed.* **2007**, *46*, 2497–2500.

(12) (a) Fu, W.-F.; Chan, K.-C.; Miskowski, V. M.; Che, C.-M. *Angew. Chem., Int. Ed.* **1999**, *38*, 2783–2785. (b) Leung, K. H.; Phillips, D. L.; Tse, M.-C.; Che, C.-M.; Miskowski, V. M. *J. Am. Chem. Soc.* **1999**, *121*, 4799–4803. (c) Fu, W.-F.; Chan, K.-C.; Cheung, K.-K.; Che, C.-M. *Chem. Eur. J.* **2001**, *7*, 4656–4664. (d) Mohamed, A. A.; Abdou, H. E.; Fackler, J. P., Jr *Inorg. Chem.* **2006**, *45*, 11–13. (e) Cheng, E. C.-C.; Leung, K.-H.; Miskowski, V. M.; Yam, V. W.-W.; Phillips, D. L. *Inorg. Chem.* **2000**, *39*, 3690–3695. (f) Fernández, E. J.; López-de-Luzuraga, J. M.; Monge, M.; Rodríguez, M. A.; Crespo, O.; Gimeno, M. C.; Laguna, A.; Jones, P. G. *Inorg. Chem.* **1998**, *37*, 6002–6006.

(13) Yam, V. W.-W.; Lo, K. K. W. *Chem. Soc. Rev.* **1999**, *28*, 323–334.

(14) (a) King, C.; Wang, J. C.; Khan, M. N. I.; Fackler, J. P., Jr *Inorg. Chem.* **1989**, *28*, 2145–2149. (b) Jaw, H.-R. C.; Savas, J. M.; Rogers, R. D.; Mason, W. R. *Inorg. Chem.* **1989**, *28*, 1028–1037. (c) Schmidbaur, H. *Angew. Chem., Int. Ed. Engl.* **1983**, *22*, 907–927.

(15) (a) Schmidbaur, H.; Mandl, J. E.; Richter, W.; Bejenke, V.; Frank, A.; Huttner, G. *Chem. Ber.* **1977**, *110*, 2236–2241. (b) Basil, J. D.; Murray, H. H.; Fackler, J. P., Jr.; Tocher, J.; Mazany, A. M.; Trzcinska-Bancroft, B.; Knachel, H.; Dudis, D.; Delord, T. J.; Marler, D. O. *J. Am. Chem. Soc.* **1985**, *107*, 6908–6915. (c) Schmidbaur, H.; Pollok, Th.; Herr, R.; Wagner, F. E.; Bau, R.; Riede, J.; Müller, G. *Organometallics* **1986**, *5*, 566–574.

(16) (a) Murray, H. H., III; Fackler, J. P., Jr.; Porter, L. C.; Mazany, A. M. *J. Chem. Soc., Chem. Commun.* **1986**, 321–322. (b) Schmidbaur, H.; Mandl, J. R.; Frank, A.; Huttner, G. *Chem. Ber.* **1976**, *109*, 466–472. (c) Usón, R.; Laguna, A.; Laguna, M.; Jiménez, J.; Jones, P. G. *J. Chem. Soc., Dalton Trans.* **1991**, 1361–1365. (d) Clark, R. J. H.; Tocher, J. H. *J. Organomet. Chem.* **1986**, *303*, 437–442. (e) Carlson, T. F.; Fackler, J. P., Jr *J. Organomet. Chem.* **2000**, *596*, 237–241.

(17) (a) Raptis, R. G.; Fackler, J. P., Jr.; Murray, H. H.; Porter, L. C. *Inorg. Chem.* **1989**, *28*, 4059–4061. (b) Dudis, D. S.; Fackler, J. P., Jr *Inorg. Chem.* **1985**, *24*, 3758–3762. (c) Raptis, R. G.; Murray, H. H.; Staples, R. J.; Porter, L. C.; Fackler, J. P., Jr *Inorg. Chem.* **1993**, *32*, 5576–5581. (d) Raptis, R. G.; Fackler, J. P., Jr.; Basil, J. D.; Dudis, D. S. *Inorg. Chem.* **1991**, *30*, 3072–3075. (e) Schmidbaur, H.; Jandik, P. *Inorg. Chim. Acta* **1983**, *74*, 97–99.

(18) (a) Raptis, R. G.; Porter, L. C.; Emrich, R. J.; Murray, H. H.; Fackler, J. P., Jr *Inorg. Chem.* **1990**, *29*, 4408–4412. (b) Mazany, A. M.; Fackler, J. P., Jr *J. Am. Chem. Soc.* **1984**, *106*, 801–802. (c) Mazany, A. M.; Fackler, J. P., Jr *J. Am. Chem. Soc.* **1984**, *106*, 801–802. (d) Raptis, R. G.; Fackler, J. P., Jr *Inorg. Chem.* **1990**, *29*, 5003–5006. (e) Fackler, J. P., Jr.; Trzcinska-Bancroft, B. *Organometallics* **1985**, *4*, 1891–1893.

(19) Méndez, L. A.; Jiménez, J.; Cerrada, E.; Mohr, F.; Laguna, M. *J. Am. Chem. Soc.* **2005**, *127*, 852–853.

(20) Cao, L.; Jennings, M. C.; Puddephatt, R. J. *Inorg. Chem.* **2007**, *46*, 1361–1368.

(21) Bhargava, S. K.; Mohr, F. *Organometallics* **2000**, *19*, 5628–5635.

(22) Qiu, Y.-X.; Wang, S.-G. *Acta Chim. Sinica* **2006**, *64*, 1416–1422.

(23) (a) Casida, M. E.; Jamorski, C.; Casida, K. C.; Salahub, D. R. J. *Chem. Phys.* **1998**, *108*, 4439–4449. (b) Statmann, R. E.; Scuseria, G. E. *J. Chem. Phys.* **1998**, *109*, 8218–8224. (c) Bauernschmitt, R.; Ahlrichs, R. *Chem. Phys. Lett.* **1996**, *256*, 454–464. (d) Frank, I. Excited State Molecular Dynamics. *SIMU Newsletter* **2001**, *3*, 63–77, Invited Review.

(24) (a) Tsipis, A. C.; Stalikas, A. V. *New J. Chem.* **2007**, *31*, 852–859. (b) Balazs, G.; Cloke, F. G. N.; Green, J. C.; Harker, R. M.; Harrison, A.; Hitchcock, P. B.; Jardine, C. N.; Walton, R. *Organometallics* **2007**, *26*, 3111–3119. (c) Kosa, M.; Karni, M.; Apeloig, Y. *Organometallics* **2007**, *26*, 2806–2814. (d) Paul, F.; da Costa, G.; Bondon, A.; Gauthier, N.; Sinbandhit, S.; Toupet, L.; Costuas, K.; Halet, J.-F.; Lapinte, C. *Organometallics* **2007**, *26*, 874–896. (e) Barakat, K. A.; Cundari, T. R.; Rabaâ, H.; Omary, M. A. *J. Phys. Chem. B* **2006**, *110*, 14645–14651. (f) Novozhilova, I. V.; Volkov, A. V.; Coppens, P. *Inorg. Chem.* **2004**, *43*, 2299–2307.

(25) O'Grady, E.; Kaltsoyannis, N. *Phys. Chem. Chem. Phys.* **2004**, *6*, 680–687.

(26) (a) Pan, Q.-J.; Zhang, H.-X. *Organometallics* **2004**, *23*, 5198–5209. (b) Pan, Q.-J.; Fu, H.-G.; Yu, H.-T.; Zhang, H.-X. *Inorg. Chem.* **2006**, *45*, 8729–8735. (c) Pan, Q.-J.; Zhou, X.; Yu, H.-T.; Zhang, H.-X.; Fu, H.-G. *Inorg. Chem. Commun.* **2007**, *10*, 183–186. (d) Pan, Q.-J.; Zhang, H.-X.; Zhou, X.; Fu, H.-G.; Yu, H.-T. *J. Phys. Chem. A* **2007**, *111*, 287–294. (e) Pan, Q.-J.; Zhang, H. X. *J. Phys. Chem. A* **2004**, *108*, 3650–3661. (f) Guo, Y.-R.; Pan, Q.-J.; Fang, G. -Z.; Liu, Z.-M. *Chem. Phys. Lett.* **2005**, *413*, 59–64.

(27) Møller, C.; Plesset, M. S. *Phys. Rev.* **1934**, *46*, 618–622.

(28) (a) Hohenberg, P.; Kohn, W. *Phys. Rev.* **1964**, *136*, B864–871. (b) Kohn, W.; Sham, L. J. *Phys. Rev.* **1965**, *140*, A1133–1138. (c) Vosko, S. H.; Wilk, L.; Nusair, M. *Can. J. Phys.* **1980**, *58*, 1200–1211.

model (PCM) in the self-consistent reaction field (SCRF)[29] method to account for the solvent effect of acetonitrile. Optimizations on **1**, **2a**, **3a**, and **4a** in the triplet excited states were performed at the unrestricted MP2 (UMP2) level. Two lower energy triplet excited states were probed for **1**, and only the lowest energy triplet excited state was studied for **2a** and **3a**; however, many attempts made to study the triplet excited states of **4a** are not successful. Herein, C_i symmetry was adopted to settle the conformations of **1** and **2** and C_2 symmetry for **3** and **4**.

We performed calculations using Hay and Wadt[30] effective core potentials (ECPs) for Au, I, Br, Cl, and P. The LANL2DZ basis sets associated with the ECPs were employed. The 6-311G* basis sets were used for the C atom. In order to better describe the molecular properties, an additional function was implemented for Au ($\alpha_f = 0.18, 1.19$), I ($\alpha_d = 0.266$), Br ($\alpha_d = 0.389$), Cl ($\alpha_d = 0.514$), and P ($\alpha_d = 0.34$).[3,7,26] Therefore, two types of basis sets, with one and two Au f functions, respectively, were used in the calculations. All the calculations were carried out by using the Gaussian03 program package.[29]

Results and Discussion

1. Ground-State Properties. a. Effects of Methods, Basis Sets, and Substituents. To test the effects of methods, basis sets, and substituents on the molecular structures, the complexes $[Au^I_2(CH_2PR_2CH_2)_2]$ (R = H (**1**), Me (**1-Me**), Ph (**1-Ph**)), in the ground states were optimized using MP2 and XαVWN methods with the 1f and 2f basis sets. In the work, the 1f and 2f basis sets refer to one and two f-type polarization functions augmented for the Au atom, respectively.

In S-Table 1 (Supporting Information), the comparison between 1f and 2f basis sets at the MP2 level indicates that the introduction of the polarization functions increases the Au−Au aurophilic attraction. The Au−Au distance calculated at the MP2-2f level is ca. 0.03−0.04 Å shorter than that at the MP2-1f level for **1**, **1-Me**, and **1-Ph**. For the methods MP2-2f and XαVWN-2f, the latter favors shorter Au−Au distances. With respect to the displacement of the R (R = Me, Et, Ph) group with the H atom, the calculated Au−Au distances at the MP2-1f level are 2.993, 2.989, and 2.963 Å for **1**, **1-Me**, and **1-Ph**, respectively, close to the experimental values of 3.023 Å for **1-Et**[15a] and of 2.977 Å for **1-Ph**.[15b] Although some differences between the calculations at the MP2-2f and XαVWN-2f levels and experimental results were found, the substituent approximation is acceptable in the paper. Therefore, the results as shown in the S-Table 1 confirm the rationality of methods, basis sets, and substituent simplifications used in the paper.

b. Geometry Structures. In this work, the geometries of eight gold complexes with different oxidation states, **1**, **2a**−**c**, **3a**,**b**, and **4a**,**b**, in the ground states were optimized at the MP2-1f, MP2-2f, and XαVWN-2f theory levels. Their structures are presented in Figure 1 with the depicted coordination orientation. Selected results from the geometry optimizations are summarized in Table 1, along with X-ray crystallographic data.[15–18]

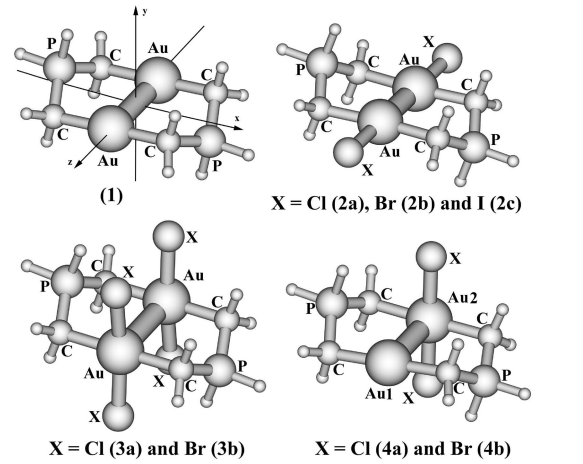

Figure 1. Structures of $[Au^I_2(CH_2PH_2CH_2)_2]$ (**1**), $[Au^{II}_2X_2(CH_2PH_2CH_2)_2]$ (X = Cl (**2a**), Br (**2b**), I (**2c**)), $[Au^{III}_2X_4(CH_2PH_2CH_2)_2]$ (X = Cl (**3a**), Br (**3b**)), and $[Au^IAu^{III}X_2(CH_2PH_2CH_2)_2]$ (X = Cl (**4a**), Br (**4b**)).

According to Table 1, similarities and differences are found between the calculated and experimental values. For **1**, the calculated Au(I)−Au(I) distance is 2.952 Å at the MP2-2f level, close to the experimental value 2.977 Å for **1-Ph**.[15b] The 3.008 Å C···C bite distance, being slightly more than the Au−Au distance, and the 90.8° C−Au−Au angle, being slightly greater than a right angle, indicate that the two Au(I) atoms tend to approach each other. As shown in Table 1, the other geometry parameters agree with the corresponding experimental values. The largest difference is ca. 0.03 Å for C−P in distances and ca. 2° for C−P−C in angles. Each Au(I) atom exhibits linear two-coordinated geometry with a 178.5° C−Au−C angle.

It is not difficult to see that, with the change in the Cl, Br, and I ligands, the corresponding geometry parameters of **2a**−**c** vary regularly (Table 1). The optimized Au−Au distances at the MP2-2f level are 2.585, 2.616, and 2.673 Å, respectively; the Au−X bond lengths of 2.402, 2.538, and 2.711 Å correspond to experimental values of 2.359, 2.516, and 2.693 Å, respectively.[16] The calculated bond lengths of Au−C and C−P fall within the range of typical values.[10,15,16] With respect to those of **1**, the oxidation results in a large change of geometry parameters for **2a**−**c**. For example, the Au−Au distance shrinks by ca. 0.37 Å on going from **1** to **2a**, the C···C distance decreases by only 0.15 Å, the C−P−C angle is reduced by ca. 8°, and the Au−C bonds are lengthened slightly (Table 1).

As seen in Table 1, the calculated geometry parameters of **3a**,**b** in all three theory levels are close to those found experimentally.[17a,b] For **3a**, the Au−Au distances fall within the range of 2.99−3.08 Å and the Au−Cl bond lengths range from 2.29 to 2.33 Å, in accordance with experimental values of 3.06 and 2.36 Å, respectively. The optimized results show that two Au atoms and two bridging phosphorus ylide ligands form an eight-membered-ring skeleton and two halide ions bond to each Au atom. Each Au atom exhibits square-planar tetracoordination with two trans halogen atoms and two trans carbon atoms from the phosphorus ylide ligands (Figure 1). Although C_2 symmetry is assumed at the beginning of the optimization, their steady-state geometries have quasi-C_{2h} symmetry. The structures of **3a**,**b** resemble those of *trans*-$[Pt_2X_4(PH_2CH_2PH_2)_2]$

(29) Frisch, M. J.; Trucks, G. W.; Schlegel, H. B.; Scuseria, G. E.; Robb, M. A.; Cheeseman, J. R.; Montgomery, J. A., Jr.; Vreven, T.; Kudin, K. N.; Burant, J. C.; Millam, J. M.; Iyengar, S. S.; Tomasi, J.; Barone, V.; Mennucci, B.; Cossi, M.; Scalmani, G.; Rega, N.; Peterson, G. A.; Nakatsuji, H.; Hada, M.; Ehara, M.; Toyota, K.; Fukuda, R.; Hasegawa, J.; Ishida, M.; Nakajima, T.; Honda, Y.; Kitao, O.; Nakai, H.; Klene, M.; Li, X.; Knox, J. E.; Hratchian, H. P.; Cross, J. B.; Adamo, C.; Jaramillo, J.; Gomperts, R.; Stratmann, R. E.; Yazyev, O.; Austin, A. J.; Cammi, R.; Pomelli, C.; Ochterski, J. W.; Ayala, P. Y.; Morokuma, K.; Voth, G. A.; Salvador, P.; Dannenberg, J. J.; Zakrzewski, V. G.; Dapprich, S.; Daniels, A. D.; Strain, M. C.; Farkas, O.; Malick, D. K.; Rabuck, A. D.; Raghavachari, K.; Foresman, J. B.; Ortiz, J. V.; Cui, Q.; Baboul, A. G.; Clifford, S.; Cioslowski, J.; Stefanov, B. B.; Liu, G.; Liashenko, A.; Piskorz, P.; Komaromi, I.; Martin, R. L.; Fox, D. J.; Keith, T.; Al-Laham, M. A.; Peng, C. Y.; Nanayakkara, A.; Challacombe, M.; Gill, P. M. W.; Johnson, B.; Chen, W.; Wong, M. W.; Gonzalez, C.; Pople, J. A. Gaussian 03, revision B.03; Gaussian, Inc.: Pittsburgh, PA, 2003.

(30) (a) Wadt, W. R.; Hay, P. J. *J. Chem. Phys.* **1985**, *82*, 284–298. (b) Hay, P. J.; Wadt, W. R. *J. Chem. Phys.* **1985**, *82*, 299–310.

Table 1. Optimized Geometry Parameters of 1−4 for the Ground States, together with the Experimental Values from X-ray Diffraction[a]

		Au−Au	Au−C	C−P	C···C	Au−X	C−Au−C	X−Au−X	C−Au−Au	C−P−C
1	MP2-1f[b]	2.993	2.122	1.792	3.019		179.3		90.4	114.8
	MP2-2f [b]	2.952	2.104	1.790	3.008		178.5		90.8	114.3
	XαVWN-2f [b]	2.948	2.047	1.769	2.997		178.6		90.7	115.8
	exptl (Ph)	2.977	2.088	1.763			179.0		89.7	113.0
2a	MP2-1f	2.645	2.134	1.780	2.878	2.407	173.7		93.1	107.9
	MP2-2f	2.585	2.117	1.778	2.857	2.402	172.6		93.7	106.9
	XαVWN-2f	2.576	2.064	1.758	2.850	2.362	172.3		93.8	108.3
	exptl (Et)	2.597	1.942	1.879		2.359				
2b	MP2-1f	2.674	2.137	1.781	2.884	2.545	174.4		92.8	108.2
	MP2-2f	2.616	2.121	1.779	2.863	2.538	173.3		93.4	107.2
	XαVWN-2f	2.603	2.066	1.758	2.857	2.505	172.9		93.5	108.7
	exptl (Ph)	2.614	2.092	1.777		2.516	173.3		92.7	106.7
2c	MP2-1f	2.723	2.140	1.782	2.895	2.717	175.4		92.3	108.6
	MP2-2f	2.673	2.126	1.780	2.877	2.711	174.5		92.8	107.8
	XαVWN-2f	2.645	2.068	1.759	2.868	2.679	173.8		93.1	109.2
	exptl	2.650				2.693				
3a	MP2-1f	3.050	2.145	1.798	3.017	2.334	179.1	169.9	89.6	114.0
	MP2-2f	2.996	2.131	1.797	3.006	2.325	179.7	169.1	90.1	113.5
	XαVWN	3.076	2.074	1.776	2.996	2.292	177.8	172.3	88.9	114.9
	exptl (Ph)	3.060				2.360				
3b	MP2-1f	3.046	2.151	1.798	3.020	2.481	179.3	164.6	89.7	114.2
	MP2-2f	2.989	2.138	1.797	3.007	2.471	179.5	163.6	90.2	113.6
	XαVWN-2f	3.078	2.077	1.776	3.008	2.440	178.1	167.4	89.1	115.7
	exptl (Ph)	3.075	2.135	1.810		2.426	178.6	164.3	90.1	
4a	MP2-1f	2.963	2.145/2.119	1.798/1.788	3.005	2.340	178.2/180.0	178.4	90.9/90.0	113.9
	MP2-2f	2.913	2.130/2.100	1.797/1.787	2.993	2.330	177.1/179.6	178.9	91.4/90.2	113.2
	XαVWN-2f	2.921	2.075/2.048	1.775/1.766	2.976	2.301	179.2/177.7	177.2	90.4/91.1	114.4
4b	MP2-1f	2.951	2.151/2.119	1.799/1.789	3.009	2.482	177.9/179.7	177.5	91.1/89.8	114.0
	MP2-2f	2.900	2.139/2.100	1.798/1.787	2.998	2.471	176.8/179.8	178.0	91.6/90.1	113.5
	XαVWN-2f	2.912	2.077/2.048	1.775/1.766	2.976	2.447	178.4/178.4	176.7	90.8/90.8	114.4
	exptl (Ph)	3.061	2.150/2.090	1.795		2.467	178.0	170.2		114.0

[a] Distances are given in Å and angles in deg. MP2-1f and MP2-2f refer to the MP2 method with the basis sets of Au ($\alpha_f = 0.2$) and Au ($\alpha_f = 0.2$, $\alpha_f = 1.19$). [b] Experimental results from refs 15–18.

($X = CN^-$, Cl, Br), a series of binuclear platinum(II) complexes with d^8-d^8 electronic structures found in previous studies.[26d]

It is found in Table 1 that the optimized geometry parameters of **4a**,**b** are somewhat different from experimental values.[18a] The calculated Au−Au distances at 2.90−2.96 Å deviate from the experimental values of ca. 3.06 Å.[18a] Our calculated results reveal that the ligand geometries about the Au centers are in accordance with those expected for their respective d electron counts. For **4a** at the MP2-2f level, the Au(I) center exhibits linear two-coordinated geometry with a 177.1° C−Au−C angle, while the Au(III) center is approximately square-planar, as reflected by the 179.6° C−Au−C and 178.9° Cl−Au−Cl angles.

Optimizations on the gold complexes **1**, **2a**−**c**, **3a**,**b**, and **4a**,**b** indicate that the agreement between the calculated results and experimental values is very good in most cases, with both types of methods. As stated in the literature,[3,7] this excellent agreement should be attributed to a cancellation of errors. On one hand, MP2 tends to overestimate the aurophilic interaction, but this effect is counterbalanced by the incompleteness of the basis sets (as evidenced by the large effect of adding a second f function on Au). On the other hand, XαVWN does not properly account for dispersion forces, but the systematic overbinding associated with the LDA approximation produces appropriate Au−Au distances.

c. Electronic Structures. With two- and four-electron oxidation, **2**−**4** have geometry features different from those in **1** as mentioned above. For example, the Au−Au separations of **1**, **3**, and **4** range from 2.90 to 3.05 Å, much longer than those of **2**; the Au centers exhibit linear two-coordinated and/or distorted -square-planar geometries. These are elucidated by the electronic structures of complexes. We give detailed information from the MP2-2f calculations in S-Tables 2−9 (Supporting Information), some of which are briefly illustrated in Figure 2. For the coordinated orientation of the complexes, the *z* axis goes through the two Au atoms and the Au_2C_4 unit lies in the *xz* plane, as shown in Figure 1.

As seen from the tables and figures in the Supporting Information, **1** possesses the greatest Au contribution in the frontier molecular orbitals such as the HOMO of $\sigma^*(s,d_{z^2-x^2})$ and the LUMO of $\pi(p_y)$. As stated in a number of literature reports,[3,7,25,26] **1** has a quasi-bimetallic $d^{10}-d^{10}$ electronic structure. However, because of the relativistic effects of the heavy metal (the relativistic radial contraction and energetic stabilization of the 6s and 6p shells and the relativistic radial expansion and energetic destabilization of the 5d shell),[31] some electrons transfer from the closed-shell $5d^{10}$ orbital to the original empty 6s and 6p orbitals, forming an Au $5d^{9.73}6s^{0.81}6p^{0.01}$ electronic configuration. Such a destruction of the Au closed-shell structure is one of the predominant driving forces to cause aurophilic attraction. That is, aurophilicity has a dispersion nature.[3a] The diffuse function ($\alpha = 0.2$) maximizes the Au^+ static polarizability and hence approximates the dispersion interaction. Thus, the calculated 2.993 Å Au−Au distance of **1** at the MP2-1f level agrees well with the experimental value of 2.977 Å, due to the use of the diffuse function. In addition, the compact function ($\alpha = 1.19$) is an appropriate polarization function for describing the primary covalent bonds to the gold. Indeed, the Au−C covalent bond length is improved at the MP2-2f level and is closer to the experimental value than that at the MP2-1f level when the compact function is introduced. Pyykkö and co-workers have attributed the aurophilic attraction to correlation effects, strengthened by relativistic effects.[3,7] We have predicted the Au−Au bond order of **1** to be 0.018 in the NBO calculations. This

(31) Pyykkö, P. *Chem. Rev.* **1988**, *88*, 563–594.

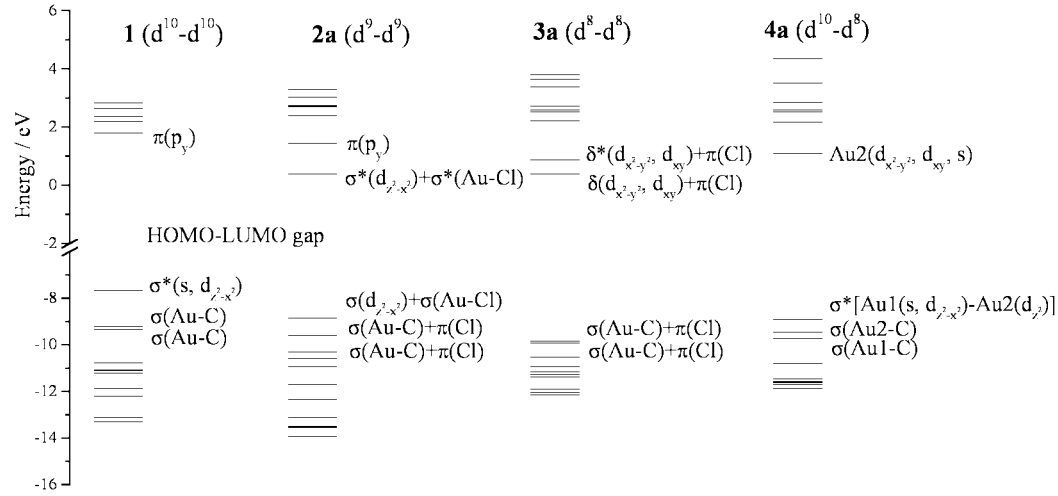

Figure 2. Energy-level diagrams of frontier molecular orbitals of **1**−**4a**.

confirms the weak aurophilic attraction. It should be emphasized that the LUMO and LUMO+1 of **1** have $\pi(p_y)$ and $\sigma(sp_z)$ characters, respectively. These are similar to the orbital arrangements of $[Au_2(SCC(CN)_2S)_2]^{2-}$ (**5a**) and $[Au_2(SC(S)S)_2]^{2-}$ (**5b**)[26f] but different from those of $[Au_2(PH_2CH_2PH_2)_2]^{2+}$ (**6**) with a LUMO of $\sigma(sp_z)$ and LUMO+1 of $\pi(p_y)$ character.[26e] Apparently, this is related to the bonding nature between the metal and ligand atoms: namely, covalent C/S−Au bonds exist in **1** and **5** and a dative P→Au bond occurs in **6**. According to previous studies,[26e,f] **5** and **6** feature the lowest energy excited states of $^3[\sigma^*(d_{z^2-x^2})\pi(p_y)]$ and $^3[\sigma^*(d_{z^2-x^2})\sigma(p_z)]$, respectively. Therefore, we conjecture that **1** should have the lowest energy $^3[\sigma^*(d_{z^2-x^2})\pi(p_y)]$ excited state, just like that of **5**.

In the process of the reaction of **1** and halide to form **2**, the bonding interactions between the $d_{z^2-x^2}$(Au) and p_z(X) orbitals remove a majority of electrons from the filled $\sigma^*(d_{z^2-x^2})$ orbitals of **1**. So **2** displays the HOMO of $\sigma(d_{z^2-x^2})+\sigma$(Au-X) and LUMO of $\sigma^*(d_{z^2-x^2})+\sigma^*$(Au-X) as shown in S-Tables 3−5 (Supporting Information). Consequently, the Au−Au distances are greatly shortened in **2** relative to that in **1**. Indeed, the Au−Au bond orders of **2a**−**c** were calculated to be 0.768, 0.721, and 0.654, respectively, far exceeding the 0.018 value for **1**. In the three complexes, the different σ-donating abilities of Cl, Br, and I result in different Au−Au distances. The calculated results show that the trend in the Au−Au distances follows the sequence Cl < Br < I, conforming to the Au−Au bond order calculations. Similar cases were found in the complexes $[Au_2X_2(SCC(CN)_2S)_2]^{2-}$ and $[Pt_2X_2(P_2O_5H_2)_4]^{4-}$ (X = I, Br, Cl).[10c,32]

In 1995, Mealli and co-workers[33] investigated some qualitative models of the weak M−M interactions between two stable square-planar units or between the L_4M and L_2M units. They found that the amount of mixing of metal p_z and s orbital characters in the critical filled MOs is of fundamental importance for the M−M interaction. That is, the stronger the σ donor capabilities of the ligands, the smaller the residual s orbital contribution and the weaker the M−M interaction will be. This conclusion supports our present calculations. In the series of complexes **2a**−**c**, the σ donor capabilities increase on going from Cl, to Br to I, which reduce Au s orbital mixing into the HOMOs on going from 6.6% to 6.0% to 4.8%. Thus, the Au−Au interactions are weakened along the complexes **2a**−**c**, reflected by the calculated Au−Au bond orders of 0.768, 0.721, and 0.654 and Au−Au distances of 2.585, 2.616, and 2.673 Å, respectively.

Because of the further two-electron oxidation, σ(Au−C) + π(X) and $\delta(d_{x^2-y^2},d_{xy})$ + π(X) contribute to the HOMO and LUMO of **3**, respectively. These are similar to the LUMO feature of $\delta(d_{x^2-y^2},d_{xy})$ of *trans*-$[Pt_2X_4(PH_2CH_2PH_2)_2]$ (X = Cl, Br).[26d] The Au−Au bond orders in **3a**,**b** are 0.034 and 0.029, respectively, suggesting a weak metal−metal bonding interaction. **4** and **2** are isoelectronic systems, except that the two halogen atoms are bonding to one gold atom in the former and two halogen atoms are bonding to two respective gold atoms in the latter. As far as the total energies of these two types of isomers are concerned, the type **4** complexes are more stable than the type **2** complexes. For example, the total energies of **4a** are 2.34 kcal/mol lower than those of **2a**. Two different chemical environments for Au atoms in **4** cause their electronic structures to differ from those of **2**; however, they very much resemble the combined properties of **1** and **3**. For example, the HOMO of **4a** is mainly contributed by 65.1% Au1 and 12.2% Au2, with the $\sigma^*[s,d_{z^2-x^2}(Au1)-d_{z^2}(Au2)]$ characters, while the LUMO mainly comes from $d_{x^2-y^2}$(Au2) + π(Cl). Like those of **1** and **3**, no single electron exists in the Au valence orbitals of **4** and the Au−Au interaction belongs to the weak metal−metal interaction, which is supported by the Au−Au bond order of ca. 0.033.

2. Spectroscopic Properties. a. Vibrational Spectra. In experimental studies, spectroscopic determination is one of the most effective means to explore the electronic structures of complexes. The binuclear gold ylide complexes $[Au^I_2(CH_2PPh_2CH_2)_2]$ and $[Au^{II}_2X_2(CH_2PPh_2CH_2)_2]$ (X = Cl, Br, I) have been studied by Raman spectroscopy.[16d,e] It was shown that the Au−Au stretching vibration was determined at 64 cm^{-1} in the Au^I complex, shifting to the higher-wavenumber region at 162, 132 and 103 cm^{-1} for X = Cl, Br and I, respectively, in the Au^{II} halogen complexes. Together the Au–X vibrations were found at 293, 220 and 165 cm^{-1}, respectively.

In this work, we performed frequency calculations for **1**−**4** at the MP2-1f, MP2-2f and XαVWN-2f theory levels. The calculated frequencies and corresponding experimental values[16d,e] are presented in S-Table 10 (Supporting Information). By

(32) (a) Woollins, J. D.; Kelly, P. F. *Coord. Chem. Rev.* **1985**, *65*, 115–140. (b) Clark, R. J. H.; Kurmoo, M.; Dawes, H. M.; Hursthouse, M. B. *Inorg. Chem.* **1986**, *25*, 409–412. (c) Alexander, K. A.; Bryan, S. A.; Fronczek, F. R.; Fultz, W. C.; Rheingold, A. L.; Roundhill, D. M.; Stein, P.; Watkins, S. F. *Inorg. Chem.* **1985**, *24*, 2803–2808.

(33) Mealli, C.; Pichierri, F.; Randaccio, L.; Zangrando, E.; Krumm, M.; Holtenrich, D.; Lippert, B. *Inorg. Chem.* **1995**, *34*, 3418–3424.

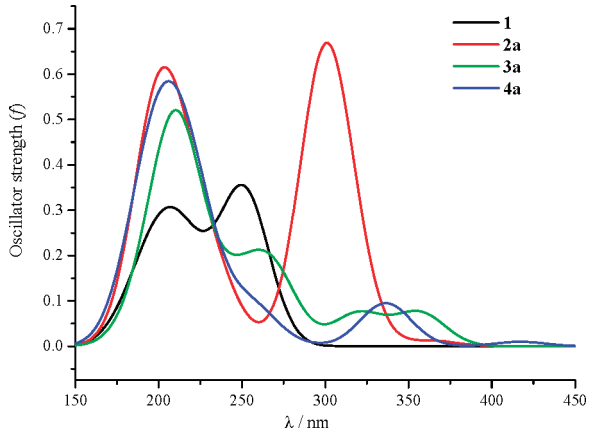

Figure 3. Simulated absorption spectra of **1**−**4a** in acetonitrile from the TD-DFT/PCM calculations.

analysis of the displacement vectors of the vibrational modes of **1**, the bands at 74−80 cm^{-1} were attributed to the Au−Au stretching vibration. These frequencies calculated at such three theory levels are ca. 10 cm^{-1} higher than the experimental value of 64 cm^{-1} for $[Au^{I}_2(CH_2PPh_2CH_2)_2]$.[16d,e] The dramatic increase in the Au−Au stretching vibrations was found for the complexes **2**. For calculations at the XαVWN-2f level, the 160, 123, and 99 cm^{-1} frequencies were assigned as the Au−Au stretching vibrations for **2a**−**c**, respectively. These agree well with the experimental values, as mentioned above. Good agreement for the Au−X vibration between the calculated and experimental results was also found. We note that the frequencies predicted at the MP2-1f and MP2-2f levels are slightly lower than those at the XαVWN-2f level. As the frequency comes from the second-order derivative of the energy, its values are inevitably affected by the energy of systems. Apparently, such frequency calculations provide evidence that a weak Au−Au bonding occurs in **1**, whereas a strong Au−Au bonding close to a single bond is formed in **2**. Similarly, we also calculated the Au−Au stretching vibrational frequencies for **3** and **4** as shown in S-Table 10.

b. Electronic Spectra. TD-DFT based on linear-response theory has recently become a reliable method for prediction of excited-state energies.[23−26] Here, the electronic transition energies of **1**−**4** were calculated using TD-DFT on the basis of optimized ground-state structures. For the MP2 optimized geometries, the TD-B3LYP method was employed, a good density functional for binuclear metal complexes indicated in our previous studies,[26c] while the TD-XαVWN method was used for the XαVWN-2f optimized ground-state structures. In combination with the PCM solvent-effect model, we obtained absorption spectra of such complexes in acetonitrile solution.

In S-Figures 1−3 (Supporting Information), we depict the simulated absorption spectra of **1**−**4** at the MP2-1f, MP2-2f, and XαVWN-2f optimized structures. Apparently, the general spectral patterns of the electronic spectra are well reproduced. The similar theoretical spectra indicate that the geometries slightly affect them. Therefore, in the following studies, we only discuss the results from the MP2-2f ground-state structures. In S-Tables 11−18 (Supporting Information), the transition energies (nm/eV) and oscillator strengths of absorptions are given. We also provide detailed MOs information in S-Tables 19−26.

In Figure 3, we have simulated the absorption spectra of **1**, **2a**, **3a**, and **4a** in acetonitrile on the basis of TD-B3LYP/PCM calculations. The theoretical spectrum of **1** contains two absorption maxima at 251 nm (4.93 eV) and 212 nm (5.84 eV). Our studies reveal these absorptions to be dominated by the

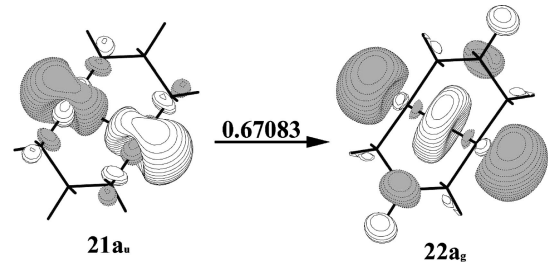

Figure 4. Single-electron transitions with |CI coefficient| >0.1 in the TD-DFT calculations for the 251 nm absorption of **1** in acetonitrile.

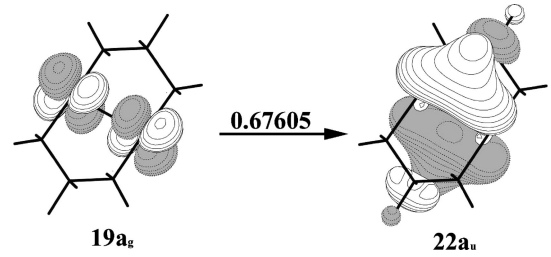

Figure 5. The single electron transitions with |CI coefficient| >0.1 in the TD-DFT calculations for the 212 nm absorption of **1** in acetonitrile.

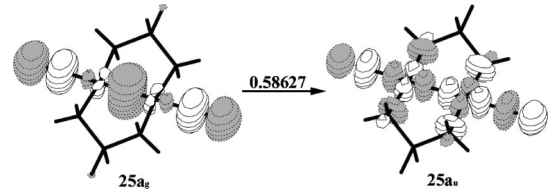

Figure 6. Single-electron transitions with |CI coefficient| >0.1 in the TD-DFT calculations for the 299 nm absorption of **2a** in acetonitrile.

metal-centered (MC) transition. Among them, the absorption at 251 nm is mainly contributed by the $21a_u \rightarrow 22a_g$ (HOMO → LUMO+1) configuration and has the largest oscillator strength of 0.337 in the absorptions, as seen in S-Table 11. In combination with S-Table 19, the absorption was attributed to a $\sigma^*(s,d_{z^2-x^2}) \rightarrow \sigma(sp_z)$ transition. In the same way, we relate the 212 nm absorption to a $\pi^*(d_{yz}) \rightarrow \pi(p_y)$ transition. To intuitively understand these electron-transition processes, we depicted the related electron density diagrams in Figures 4 and 5. Apparently, these diagrams confirm such assignments. So far, the $\sigma^*(d) \rightarrow \sigma(sp_z)$ transition absorption has been found in many binuclear gold(I) complexes in experiments. For example, $[Au^{I}_2(NRCHNR)_2]$ (R = 2,6-dimethylphenyl),[12d] $[N(PPh_3)_2]_2[Au^{I}_2(SC(S)S)_2]$,[12e] and $[Au^{I}_2(PCy_2CH_2PCy_2)_2](ClO_4)_2$[12a] show strong absorption bands at 255, 314, and 278 nm, respectively, which have been attributed to the $\sigma^*(d) \rightarrow \sigma(sp_z)$ transitions.

With respect to **2a**, the stimulated absorption spectrum is dominated by two absorption maxima at 299 nm (4.15 eV) and 203 nm (6.10 eV), as shown in Figure 3. The $25a_g \rightarrow 25a_u$ (HOMO → LUMO) transition contributes to the lower energy absorption at 299 nm with an oscillator strength of 0.582 as seen in S-Table 12. The absorption corresponds to a $\sigma(d_{z^2-x^2})+\sigma(Au-Cl) \rightarrow \sigma^*(d_{z^2-x^2})+\sigma^*(Au-Cl)$ transition, reflected by Figure 6 and S-Table 20.

It is seen from Figure 3 that the stimulated absorption spectrum of **3a** is relatively complicated, displaying four peaks at 357, 319, 266, and 211 nm. The molecular orbitals and

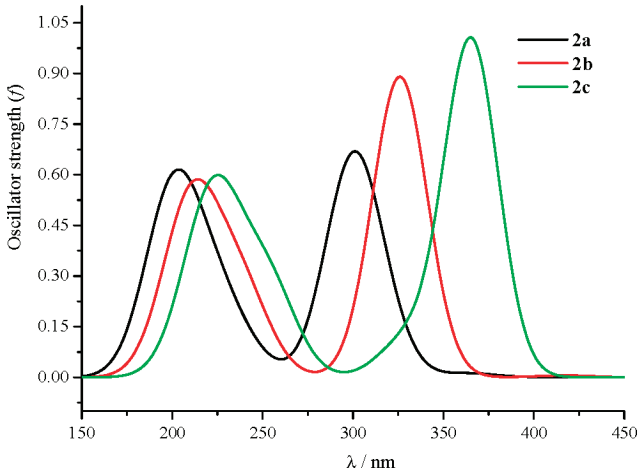

Figure 7. Simulated absorption spectra of **2a**−**c** in acetonitrile from TD-DFT/PCM calculations.

electronic transitions of **3a** presented in S-Tables 15 and 23 indicate that the electron is mainly excited into the 29a (LUMO) and 30a (LUMO+1) orbitals. The two orbitals have $\delta(d_{x^2-y^2},d_{xy})$ and $\delta^*(d_{x^2-y^2},d_{xy})$ characters mixed with π(Cl) composition, respectively. The 357 and 319 nm absorptions were attributed to the σ(Au−C) → $\delta(d_{x^2-y^2},d_{xy})$ and σ(Au−C) → $\delta^*(d_{x^2-y^2},d_{xy})$ charge transfer transitions, respectively. The other two bands mainly come from π(Cl) → $\delta(d_{x^2-y^2},d_{xy})$ electronic transitions.

Because the two gold atoms in **4a** have different chemical environments, they exhibit peculiar electronic properties relative to the isoelectronic **2a**. As stated above, **4a** has the combined features of **1** and **3a** in both geometry and electronic structures. S-Table 25 shows that the HOMO (25a) has 65.5% Au1 and 17.8% Au2 characters, forming a σ^* bond. The LUMO (26a) is mainly contributed by $d_{x^2-y^2}$ and d_{xy} of Au2, and the LUMO+1 (27a) is composed of the two gold atoms with $\sigma(sp_z)$ bonding. We can see from S-Table 17 that the lowest energy 417 nm (2.97 eV) absorption arising from the 25a → 26a electronic configuration is the $\sigma^*[s,d_{z^2-x^2}(Au1)-d_{z^2}(Au2)]$ → $d_{x^2-y^2},d_{xy}(Au2)$ transition, similar to that of **3a**; however, the 25a → 27a excitation configuration gives rise to a 224 nm absorption (oscillator strength of 0.180) with the $\sigma^*[s,d_{z^2-x^2}(Au1)-d_{z^2}(Au2)]$→$\sigma(sp_z)$ characters, just like that in **1**. In fact, the complex **4a** with mixed-valence Au(I)/Au(III) could correspond to heterobimetallic $d^{10}-d^8$ complexes such as Au(I)−M(II) (M = Pt, Pd, Ni)[34] and Au(I)−M(I) (M = Ir, Rh).[35] In experiments on these complexes, the $\sigma^*(d_{z^2})$ → $\sigma(sp_z)$ absorption bands were found to have larger molar absorption coefficients, supporting our present study.

In Figure 7 we depict the simulated spectra of **2a**−**c**. With the variation from Cl, Br, I ligands, the two intense peaks shift to longer wavelength. Similar cases have been observed for many complexes such as $[Au_2X_2(SCC(CN)_2S)_2]^{2-}$ and $[Pt_2X_2(P_2O_5H_2)_4]^{4-}$ (X = Cl, Br, I) in experiments.[10c,32] For instance, the gold complexes $[Au_2X_2(SCC(CN)_2S)_2]^{2-}$ (X = Cl, Br, I) exhibit intense absorption bands at 550, 586, and 640 nm in acetonitrile solution, respectively.[10c] In our previous theoretical studies on $[Pt_2X_2(P_2O_5H_2)_4]^{4-}$,[26c] the two featured absorptions observed in experiments are well reproduced by the theoretical calculations. We attributed the lowest energy absorption to the admixture of $\sigma(d_{z^2})$ → $\sigma^*(d_{z^2})$ and σ(Pt−Cl) → σ^*(Pt−Cl) transitions. The shifting trend of three platinum(III) complexes was rationalized by the diagrams of the electronic structures. Herein, a similar case occurs for **2a**−**c**. For example, the lower energy absorptions calculated at 299, 327, and 365 nm for **2a**−**c**, respectively, all arise from the $25a_g$(HOMO) → $25a_u$(LUMO) configuration. Along the change from Cl to Br to I, the energy of the HOMO increases but the LUMO is stabilized. This is clearly correlated with the partition of halide, as seen in S-Tables 20−22. In addition, we give the simulated spectra of **3a**,**b** and **4a**,**b** in S-Figures 4 and 5, respectively. Detailed information on the electronic transitions is presented in S-Tables 15−18 and 23−26. We also depict the electron density diagrams of their featured transitions in S-Figures 6−9.

3. Excited-State Properties. A theoretical understanding of the excited-state properties of binuclear gold complexes with different oxidation states serves as a foundation to develop their potential applications such as luminescent materials and devices and to design novel molecules. In this work, the UMP2 method was used to optimize structures of **1** and its chloride derivatives (**2a**, **3a**, and **4a**) in the triplet excited states. The frequency calculations reveal that the lower energy excited-state structures of **1**, **2a**, and **3a** are true minima on the potential energy surface, while that of **4a** is a transition state with an imaginary frequency of −107 cm^{-1}. Many attempts made on **4a** to look for the steady triplet excited-state structure have been unsuccessful. In Table 2, the geometry parameters optimized at the UMP2-2f theory level are given.

In the UMP2 calculations on **1**, two triplet excited states, ^3A_g and ^3A_u, were found. The former is lower in energy than the latter. For the lower energy ^3A_g excited state, calculations show that the Au−Au distance shrinks by ca. 0.34 Å on going from the ground state to the triplet excited state, the C···C distance decreases by ca. 0.11 Å, and the Au−C bond lengths remain constant (Tables 1 and 2). Because the shrinkage of Au−Au is much more than that of C···C, the bonding interaction between the two Au atoms drives the Au−Au shrinkage. A similar case was found for the ^3A_u excited state, in which the Au−Au distance and C···C bite distance are reduced relatively little, by ca. 0.26 and 0.03 Å, respectively. Analyses of their electronic structures reveal that the ^3A_g and ^3A_u excited states are produced by the promotion of electrons from the $\sigma^*(d_{z^2-x^2})$ antibonding orbital to the $\pi(p_y)$ and $\sigma(sp_z)$ bonding orbitals, respectively. Because their HOMOs have bonding characters, the Au−Au distances are strongly shortened. We can understand these processes by the electron density diagrams of their HOMOs and LUMOs, presented in Figure 8. It is worth noting that the Au−Au distances in the triplet excited states of **1** are very close to those of **2a**−**c** in the ground states. Figures 2 and 7 illustrate that these Au−Au interactions have a bonding nature but have different origins.

Over the last two decades, many attempts to predict the metal−metal distance in the triplet excited state have been made in experiments. For example, through Franck−Condon analy-

(34) (a) Xia, B.-H.; Zhang, H.-X.; Che, C.-M.; Leung, K.-H.; Phillips, D. L.; Zhu, N.; Zhou, Z.-Y. *J. Am. Chem. Soc.* **2003**, *125*, 10362–10374. (b) Stork, J. R.; Rios, D.; Pham, D.; Bicocca, V.; Olmstead, M. M.; Balch, A. L. *Inorg. Chem.* **2005**, *44*, 3466–3472. (c) Crespo, O.; Laguna, A.; Fernández, E. J.; López-de-Luzuriaga, J. M.; Jones, P. G.; Teichert, M.; Monge, M.; Pyykkö, P.; Runeberg, N.; Schütz, M.; Werner, H.-J. *Inorg. Chem.* **2000**, *39*, 4786–4792. (d) Yip, H.-K.; Lin, H.-M.; Cheung, K.-K.; Che, C.-M.; Wang, Y. *Inorg. Chem.* **1994**, *33*, 1644–1651.

(35) (a) Esswein, A. J.; Dempsey, J. L.; Nocera, D. G. *Inorg. Chem.* **2007**, *46*, 2362–2364. (b) Yip, H.-K.; Lin, H.-M.; Wang, Y.; Che, C.-M. *Inorg. Chem.* **1993**, *32*, 3402–3407. (c) Striplin, D. R.; Crosby, G. A. *J. Phys. Chem.* **1995**, *99*, 7977–7984.

Table 2. Optimized Geometry Parameters of 1, 2a, and 3a using the UMP2-2f Method for the Triplet Excited State[a]

	excited state	Au−Au	Au−C	C−P	C···C	Au−X	C−Au−C	X−Au−Au	X−Au−X	C−Au−Au	C−P−C
1	^3A_g	2.608	2.103	1.783	2.897		172.1			94.0	108.7
	^3A_u	2.690	2.106	1.792	2.980		172.1			94.0	112.5
2a	^3A_u	2.867	2.120	1.790	3.004	2.473	174.7	74.6		89.0/94.6	114.0
3a	^3B	2.873	2.149	1.789	2.954	2.381	177.8	93.5	173.1	91.1	111.3

[a] Distances in are given in Å and angles in deg.

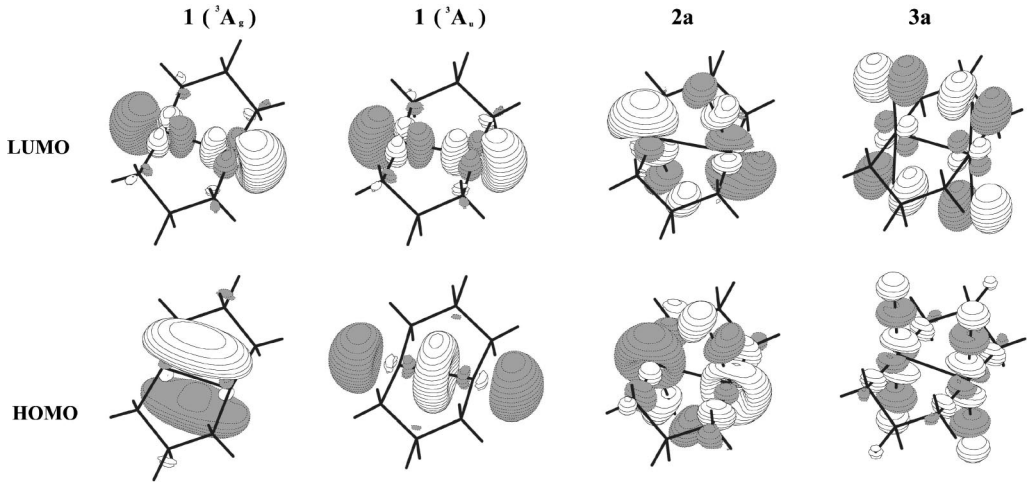

Figure 8. Electron density diagrams of HOMO and LUMO for **1**, **2a**, and **3a** from UMP2 calculations.

sis,[36] resonance Raman spectra,[37] microsecond-resolved XAFS,[38] and time-resolved X-ray diffraction,[39] the authors summarized that the Pt−Pt distances of $Y_n[Pt_2(P_2O_5H_2)_4]$ (Y = K^+, $(n\text{-}Bu_4N)^+$, Ba^{2+}, $(Et_4N)_3H^{4+}$) in the $^3[\sigma^*(d_{z^2})\sigma(p_z)]$ excited state contract ca. 0.21−0.29 Å relative to that in the ground state. A similar predication was made on homobinuclear $[Au^I_2(PCy_2CH_2PCy_2)_2]^{2+}$ [12a–c] and heterobinuclear $[Au^IPt^{II}(CN)_2(PCy_2CH_2PCy_2)_2]^{2+}$.[34a] These experimental studies support our present study on **1**.

As discussed in Electronic Structures, the bonding nature between the metal and ligand atoms plays a significant role in determining the lowest energy excited-state origin of binuclear gold(I) complexes. Namely, **1** and **5** with C/S−Au covalent bonds feature the lowest energy $^3[\sigma^*(d_{z^2-x^2})\pi(p_y)]$ excited state, while **6** with a P→Au dative bond favors the $^3[\sigma^*(d_{z^2-x^2})\sigma(p_z)]$ state. A spectroscopic experiment by Fackler et al. showed that the complex $[Au^I_2(CH_2PPh_2CH_2)_2]$ exhibits phosphorescent emission at 483 nm at room temperature in the solid state.[14a] We attributed the emission to the $^3[\sigma^*(d_{z^2-x^2})\pi(p_y)]$ origin, different from the assignment for the emission of **6**.

Just like the case in **1**, optimizations on **3a** at the UMP2 level show that the Au−Au distance shortens by ca. 0.12 Å upon excitation, the C···C distance decreases by ca. 0.05 Å, and the Au−C bonds lengthen ca. 0.02 Å (Tables 1 and 2). Although **3a** and **1** have similar structural variations upon excitation, their excited-state origins differ greatly. As shown in Figure 8, the triplet excited state of **3a** has $\delta(d_{x^2-y^2})$ and $\pi^*(d_{yz})$ characters for the HOMO and LUMO, respectively. As the $\delta(d_{x^2-y^2})$ bonding interaction is relatively weaker than the $\sigma(sp_z)$ and $\pi(p_y)$ bondings, the Au−Au contraction of **3a** is less than that of **1**. Optimizations on **2a** at the UMP2 level reveal that it has different excited-state characteristics. The Au−Au distance changes from 2.585 Å in the ground state to 2.867 Å in the triplet excited state; the chloride atom deviates greatly from its original position, reflected by the Cl−Au−Au angles of 74.6° in the excited state and 180° in the ground state. Because the electron is excited into the antibonding orbital of **2a**, as shown in Figure 8, the Au−Au distance lengthens greatly.

Such analyses on the excited-state electronic structures of **1**, **2a**, and **3a** indicate that the geometrical change from the ground state to the excited state is closely related to the HOMO with metal−metal character: i.e. the orbital to which an electron has been transferred. In fact, the nature of the depopulated orbital is also important for the geometrical change. For instance, the LUMOs of **1** in ^3A_g and ^3A_u excited states both have the $\sigma^*(d_{z^2-x^2})$ characters while their HOMOs come from $\pi(p_y)$ and $\sigma(sp_z)$ contributions, respectively. The geometrical changes from the ground state to the ^3A_g and ^3A_u excited states are mainly contributed by the LUMO → HOMO configuration, corresponding to the $\sigma^*(d_{z^2-x^2}) \rightarrow \pi(p_y)$ and $\sigma^*(d_{z^2-x^2}) \rightarrow \sigma(sp_z)$ transition properties, respectively. In general, the $\sigma(sp_z)$ bonding interaction should be stronger than the $\pi(p_y)$ bonding interaction. In other words, the larger Au−Au contraction should be found in the $^1A_g \rightarrow {}^3A_u$ state−state transition. However, the UMP2 optimizations show that the $^1A_g \rightarrow {}^3A_g$ state−state transition results in a larger contraction than the $^1A_g \rightarrow {}^3A_u$ transition does. To analyze the wavefunctions of the ^3A_g and ^3A_u excited states, we found ca. 56.5% and 60.2% Au $d_{z^2-x^2}$ contributions to the LUMOs (σ^* antibonding), respectively. The smaller $\sigma^*(d_{z^2-x^2})$ contribution to the ^3A_g excited state favors the shorter excited-state Au−Au distance and thus leads to a larger Au−Au contraction on going from the ground state to the excited state.

(36) (a) Fordyce, W. A.; Brummer, J. G.; Grosby, G. A. *J. Am. Chem. Soc.* **1981**, *103*, 7061–7064. (b) Rice, S. F.; Gray, H. B. *J. Am. Chem. Soc.* **1983**, *105*, 4571–4575. (c) Brummer, J. G.; Crosby, G. A. *Chem. Phys. Lett.* **1984**, *112*, 15–19.

(37) (a) Leung, K. H.; Phillips, D. L.; Che, C.-M.; Miskowski, V. M. *J. Raman Spectrosc.* **1999**, *30*, 987–993. (b) Che, C.-M.; Butler, L. G.; Gray, H. B.; Crooks, R. M.; Woodrusff, W. H. *J. Am. Chem. Soc.* **1983**, *105*, 5492–5494.

(38) Thiel, D. J.; Līvinš, P.; Stern, E. A.; Lewis, A. *Nature* **1993**, *362*, 40–43.

(39) Kim, C. D.; Pillet, S.; Wu, G.; Fullagar, W. K.; Coppens, P. *Acta Crystallogr.* **2002**, *A58*, 133–137.

Conclusions

The electronic structures and spectroscopic properties of **1**−**4** were investigated by the combined ab initio and density functional theory methods. The effects of methods, basis sets and substituents were considered to confirm our calculations. Three remarkable points were emphasized as follows.

Electronic Structures. The HOMO and LUMO of **1** feature the $\sigma^*(s,d_{z^2-x^2})$ and $\pi(p_y)$ characters, respectively. The two- and four-electron oxidations of **1** with halide form **2** and **3**, respectively. Consequently, the HOMO and LUMO of $\sigma(d_{z^2-x^2})$ and $\sigma^*(d_{z^2-x^2})$ were found for **2** and $\sigma(Au-C) + \pi(X)$ and $\delta(d_{x^2-y^2}, d_{xy}) + \pi(X)$ for **3**, respectively. When the two-electron oxidation is limited to one gold center for **1**, complex **4** with two gold atoms in different chemical environments is produced. Its electronic structures resemble the combined properties of **1** and **3**. The electronic properties of **1**−**4** confirm their different geometrical features that the Au centers are linear two-coordinated and/or distorted square-planar.

Metal−**Metal Interactions.** The geometry optimizations, bond order, and frequency calculations reveal that weak Au−Au bonding was found in **1**, **3** and **4**, while an approximate Au−Au single bond was found in **2**. It is the oxidation of **1** with halide that removes the electrons of the $\sigma^*(d_{z^2-x^2})$ orbital to result in the occurrence of an Au−Au σ single bond in **2**. Due to the different donor strengths of halogen atoms, the Au−Au distances in **2a**−**c** follow the sequence Cl < Br < I, conforming to the bond-order and frequency calculations. Upon excitation, the excited states of $^3[\sigma^*(d_{z^2-x^2})\pi(p_y)]$ and $^3[\sigma^*(d_{z^2-x^2})\sigma(p_z)]$ of **1** possess ca. 2.61 and 2.69 Å Au−Au distances, respectively, closer to the single bonding. Although the Au−Au interactions present in the ground states of **2** and the excited states of **1** are closer to the Au−Au σ single bonding, they have different origins.

Electronic Spectroscopy. The TD-DFT/PCM calculations reveal that the intense absorptions of **1** are dominated by metal-centered transitions such as $\sigma^*(s,d_{z^2-x^2}) \rightarrow \sigma(sp_z)$ and $\pi^*(d_{yz}) \rightarrow \pi(p_y)$. However, the intense lower energy peaks of **2** arise from $\sigma(d_{z^2-x^2}) \rightarrow \sigma^*(d_{z^2-x^2})$, similar to those found in $[Au_2X_2(SCC(CN)_2S)_2]^{2-}$ and $[Pt_2X_2(P_2O_5H_2)_4]^{4-}$ (X = Cl, Br, I).[10c,32] The electronic transitions of **3** are clearly related to excitation into the $\delta(d_{x^2-y^2},d_{xy})$ and $\delta^*(d_{x^2-y^2},d_{xy})$ orbitals. As expected, **4** has the combined charge transfer features of **1** and **3**. The results of **4** with mixed-valence Au(I)/Au(III) provide the theoretical evidence for the spectroscopic assignments of heterobimetallic Au(I)−M(II) (M = Pt, Pd, Ni)[34] and Au(I)−M(I) (M = Ir, Rh).[35]

Acknowledgment. This work was supported by the Key Program Projects of National Nature Science Foundation of China (No. 20431030), the Natural Science Foundation of China (Nos. 20703015, 20573042, and 20671032), the Progamme for New Century Excellent Talents in University (No. NCET-04-0341), the Natural Science Foundation of Heilongjiang Province of China (No. B200601), the Science Foundation for Excellent Youth of Heilongjiang University of China (No. JC2006L2), and the supporting plan for Excellent Youth of Common Universities of Heilongjiang province of China (No. 1153G028).

Supporting Information Available: Tables giving optimized ground-state geometries of **1**, **1-Me**, and **1-Ph**, calculated Au−Au and Au−X stretching vibrational frequencies of **1**−**4**, partial molecular orbital contributions (%) for **1**−**4** in the ground state from MP2-2f calculations, and partial molecular orbital contributions (%) for **1**−**4** in acetonitrile solution from TD-DFT (B3LYP) calculations and figures giving simulated absorption spectra for **1**−**4** on the basis of MP2-1f, M2-2f, and XαVWN-2f optimized geometries, simulated absorption spectra for **3** and **4** on the basis of M2-2f optimized geometries, and electron density diagrams of **3** and **4**. This material is available free of charge via the Internet at http://pubs.acs.org.

OM701114Z